BULLETIN OF THE EARTHQUAKE
RESEARCH INSTITUTE
Vol. 47 (1969), pp. 673-700

# 29. *Numerical Experiments for the Tsunami Propagation— the 1964 Niigata Tsunami and the 1968 Tokachi-oki Tsunami.*

By Isamu AIDA,

Earthquake Research Institute.

(Read Jan. 28, 1969.—Received May 30, 1969.)

## Abstract

The present work is an attempt to approach the problem of tsunami propagation by means of a numerical experiment. A preliminary experiment to examine the computing accuracy has been carried out for the square origin in a uniform water depth with a sufficient performance. The Niigata tsunami was treated, because the submarine crustal movement in the tsunami origin had been surveyed in detail. The experimental results were satisfactory in the comparison of the wave forms with two tide gage records and also in the comparison of profile of the maximum water elevation with the actual inundation height. The energy radiation pattern of the wave origin itself shows the directivity of such a shape as an Arabic numeral, 8, however, the actual tsunami radiates the strong energy toward the coast but the weak energy seaward. It is understood that this is caused by a refraction of wave on the sloping shelf. As for the Tokachi-oki tsunami, several models of wave origin were assumed for experiments. By comparing the computed result with tide gage records, the most probable model was selected.

## 1. Introduction

Most theoretical studies for a tsunami generation have been confined to such simplified models as analytical calculations were possible, and also most problems for a propagation have been solved for a simple topography. In actual tsunamis, however, their generating areas and propagating paths exist on the continental shelf or slope where water depth varies widely. The interaction of waves reflected from the coast and reflected partially on the shelf is so complicated that it can not be treated analytically. Therefore, it is very difficult to compare directly the behaviour of the actual tsunami with the theoretical one. Although a hydraulic model experiment is an important way to fill the gap, the construction of a large, elaborate model and measurement with sufficient accuracy will require considerably more expense and a long period of

time for the work. Recently, as electronic computers were widely used, a numerical experiment became easier. As for the numerical experiment of water waves, the problem of storm surge in a bay had already reached such a stage that a fairly precise discussion could be made. As for the tsunami propagation, several studies were carried out for large bays, such as Tokyo bay [*Isozaki and Unoki*, 1964] and Ofunato bay [*Fukuchi and Ito*, 1966, and *Ito, Tanimoto and Kihara*, 1969]. The Chilean tsunami traveling over the Pacific ocean was also treated by *Ueno* [1965]. However, the tsunami propagation from a generating area on the continental shelf and slope has not been treated yet.

The writer, in this paper, attempts the numerical experiment for the Niigata tsunami of 1964, because this tsunami is a valuable example in that the submarine crustal movement in the vicinity of tsunami origin was surveyed in detail. And also, on the Tokachi-oki tsunami of 1968, similar computations with respect to several models of tsunami origin are carried out to estimate a crustal deformation in the generating area consistent with observed tsunami records.

## 2. Method of the numerical experiment

In the present method of numerical experiment, difference equations transformed from basic differential equations are numerically integrated step by step. The basic equations of motion are

$$\left.\begin{aligned}\frac{\partial u}{\partial t}&=-g\frac{\partial \zeta}{\partial x}\,,\\ \frac{\partial v}{\partial t}&=-g\frac{\partial \zeta}{\partial y}\,,\end{aligned}\right\} \tag{1}$$

where $u$ and $v$ are the velocity components in the directions of the coordinates, $x$ and $y$, $\zeta$ is the water level elevation relative to still water and $g$ is the acceleration of gravity. The Corioli's force is neglected because the period of waves considered is relatively small. The frictional force due to viscosity is neglected, because a deep sea region is mainly treated in this case.

In terms of $q_x$ and $q_y$ which are the vertically integrated components of the transport in a small width $b$, the equation (1) is transformed into

$$\left.\begin{aligned}\frac{\partial q_x}{\partial t}&=-gbh\frac{\partial \zeta}{\partial x}\,,\\ \frac{\partial q_y}{\partial t}&=-gbh\frac{\partial \zeta}{\partial y}\,,\end{aligned}\right\} \tag{2}$$

where $h$ is a water depth, and $\zeta/h \ll 1$ is assumed.

The equation of continuity is

$$\frac{\partial \zeta}{\partial t} = -\frac{1}{b}\left(\frac{\partial q_x}{\partial x} + \frac{\partial q_y}{\partial y}\right). \qquad (3)$$

Taking into consideration a uniform Cartesian mesh at spacing, $\Delta s$, for uniform time steps, $\Delta t$, (Fig. 1), the equations (2) and (3) are rewritten to the following difference equations,

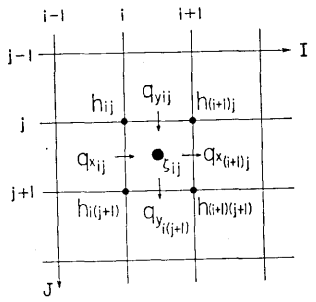


Fig. 1. Scheme for computed variables.

$$\left.\begin{aligned} q_{xij}(t+\Delta t) &= q_{xij}(t) - (\Delta t)g\frac{h_{ij}+h_{i(j+1)}}{2}\left[\zeta_{ij}\left(t+\frac{\Delta t}{2}\right) - \zeta_{(i-1)j}\left(t+\frac{\Delta t}{2}\right)\right], \\ q_{yij}(t+\Delta t) &= q_{yij}(t) - (\Delta t)g\frac{h_{ij}+h_{(i+1)j}}{2}\left[\zeta_{ij}\left(t+\frac{\Delta t}{2}\right) - \zeta_{i(j-1)}\left(t+\frac{\Delta t}{2}\right)\right], \end{aligned}\right\} \qquad (4)$$

and

$$\begin{aligned} \zeta_{ij}(t+\Delta t) = \zeta_{ij}(t) - \frac{\Delta t}{(\Delta s)^2}\Big[ & q_{x(i+1)j}\left(t+\frac{\Delta t}{2}\right) - q_{xij}\left(t+\frac{\Delta t}{2}\right) \\ & + q_{yi(j+1)}\left(t+\frac{\Delta t}{2}\right) - q_{yij}\left(t+\frac{\Delta t}{2}\right)\Big]. \end{aligned} \qquad (5)$$

From the equations (4) and (5), we can alternately compute the distribution of $\zeta$ and those of $q_x$ and $q_y$.

*Initial conditions*:

If the crustal movement occurred instantaneously in the tsunami originating area, the disturbance which is completely identical with the shape of the submarine crustal deformation is generated on the sea surface just over the deformed bottom. As the first approximation, therefore, the elevation of sea surface in the tsunami originating area was given as the initial condition to resolve the present problem, instead of the bottom deformation.

*Boundary conditions*:

There are two kinds of boundaries in the computation, namely, one is a boundary between the sea and the land, another is the seaward border of a computing area. In the former, the transport, $q_x$ or $q_y$, normal to the coast is put zero. In the latter, the formula analogous to the relation between the water elevation and the transport of progressive waves,

$$q_x \quad \text{or} \quad q_y = \pm(\Delta s)\sqrt{gh}\zeta\,, \qquad (6)$$

is assumed, where the sign "$\pm$" is decided as $q_x$ or $q_y$ flows out from the computational region when $\zeta$ is positive. Such a boundary condition was employed with a sufficient performance in the numerical computation on storm surges by *Reid and Bodine* [1968]. We also confirmed that computed results were little disturbed by the effect of seaward boundary.

*Computation stability*:
To make a stable computation,

$$(\Delta s/\Delta t) > \sqrt{2gh_{max}} \tag{7}$$

is required, where $h_{max}$ is the maximum water depth in a calculating region. As will be mentioned in a later section, weak oscillations occur in process of a numerical computation, despite the condition (7). To suppress the oscillations, all of $\zeta$, $q_x$ and $q_y$ are averaged for the computing point and neighbouring four points with the weight of 1/10.

## 3. Square origin in the sea of a uniform depth

To examine the accuracy of a computation, a preliminary experiment for a square origin is carried out. In the experiment, the water depth is uniformly 50 m deep, the water elevation of 1m is supposed for the wave origin in which a side of square is 50 km long. As shown in Fig. 2, two cases of different grid intervals are treated, the one is of 10 km spacing, equivalent to 6 grid points on one side and the other of 3.85km spacing, equivalent to 14 grid points on one side. The values of water elevation $\zeta$ are evaluated on $22 \times 25$ grid points for uniform time steps, 0.2min, and only the values at the points shown by open circles in Fig. 2 are printed at a time interval of 1min. The wave forms at the typical points are shown in Fig. 3, where $O$ and $O'$ are the center of wave origin and $A, B, C$ and $D$ or $A', B', C'$ and $D'$ are the points on a circle closely surrounding the wave origin. The results in the case of coarse spacing grid are shown at the left side in the figure and that of fine spacing grid at the right.

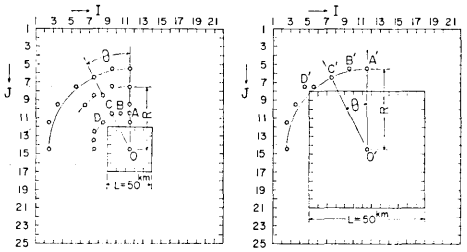


Fig. 2. Computing grid scheme for the experiment on the square origin. The left side is the case of a coarse grid spacing and the right a fine grid spacing. Computing results were printed in points shown by open circles.

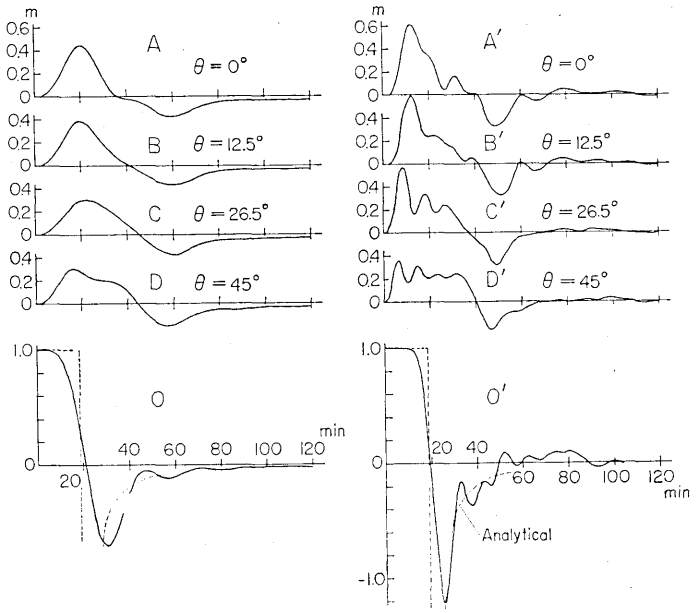


Fig. 3. Wave forms on the circle closely surrounded the square origin. Alphabetical characters correspond to the marks of points as shown in Fig. 2. A solution by means of an analytical method is shown by a broken line only for the water elevation in the center of origin.

Comparing the latter results with the former, the shape of initial rise is steeper and the oscillations of the period of 8 to 10 minutes appear. If the oscillations were filtered, the wave form agrees considerably well with the former case, namely, as far as the fundamental wave is of interest, both forms are very similar. The short period oscillations appearing in the case of fine spacing grid are caused in the course of numerical integration and attenuate gradually from the beginning of waves, as time passes.

The wave form at the center of a square wave origin can be calculated easily from the wave equation by using Green's function [*Kajiura*, 1963]. The curve in Fig. 4 or shown by broken lines in Fig. 3 is the result obtained by this method (see Appendix). A long wave velocity, $c$, is equal to 1330 m/min and the distance from the center of

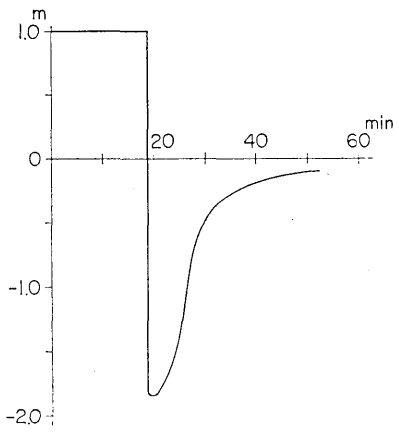


Fig. 4. Water elevation in the center of origin solved analytically by means of using Green's function.

origin to a side, $L/2$, is equal to 25 km, thus the initial water elevation, given to be 1 m, is held till $t=L/2c=18.6$ min and descends instantaneously to $-1.83$ m at that time. After the minimum elevation appeared at $t=20$ min, the elevation goes back gradually near zero and recovers to $-0.1$ m at $t=50$ min. The values obtained by the numerical experiment coincides well with the analytical solution, except for the portion of negative large values. Namely, in the numerical experiment, sufficient accuracy can be expected, if the grid spacing was taken considerably small and the oscillations caused by the process of numerical computations were reduced. However, even if the grid spacing is relatively coarse, the experiment will bring sufficient practical value as far as the fundamental wave of long period is concerned. It is qualitatively apparent that the results of numerical computation are equivalent to the low pass filtering with the cut-off frequency determined from the wave length as long as twice a grid spacing $\Delta s$. In the present case, the cut-off period is about 15 min for the coarse spacing grid, and about 6min for the fine spacing grid.

We shall hereafter develop the investigation of the problem confined to the comparative long period wave, taking into account the limitation due to a spacing of grid.

The characteristics of a square origin obtained by this experiment are explained in the following. The directivity of wave radiations is clearly recognized in the circumference near a wave origin, however, in

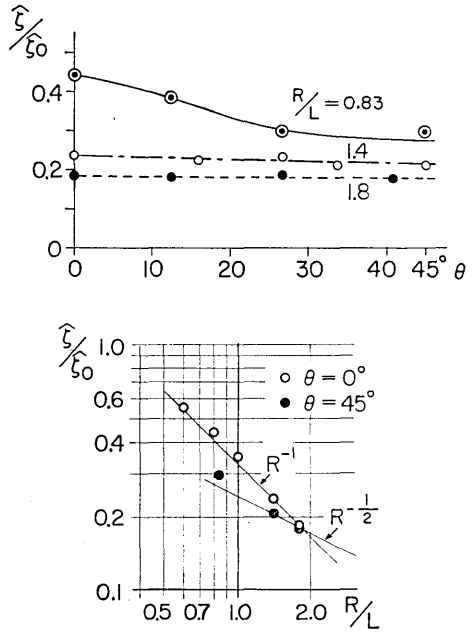


Fig. 5. Directivity (upper) and attenuation (lower) of waves radiated outward from a square origin. $\hat{\zeta}_0$ is height of water elevation given to a wave origin and $\hat{\zeta}$ the maximum amplitude of elavation in various points.

the place distant roughly the length of a side from a margin of origin, it hardly appears at all. The upper graph in Fig. 5 shows this fact. Near the wave origin, $R/L=0.83$, where $R$ is the distance measured from the center of wave origin, the amplitude of waves in the direction of diagonal line, $\theta=45°$, is 0.65 times the one normal to a side, $\theta=0°$. When $R/L$ is equal to 1.4 or 1.8, the difference of wave amplitudes between the direction $\theta=0°$ and 45° is hardly recognized.

The attenuation of amplitude for a distance is shown in the lower part of Fig. 5. In $R/L<2.0$, the wave amplitudes are inversely proportional to the root of $R$ in the direction $\theta=45°$, and to $R$ in the direction $\theta=0°$. The directivity fades out in about $R/L=2.0$ by the difference of attenuation.

## 4. The Niigata tsunami of 1964

A great earthquake with magnitude 7.5 (J.M.A.) occurred on June 16, 1964. Its epicenter was located at the south of Awa Shima Island in Niigata prefecture. The tsunami which accompanied it attacked the coast along the Japan Sea. The maximum inundated height reached as high as 6m near the center and the height was rapidly reduced as it parted north and south-wards from there. From the travel times of the tsunami, the tsunami originating area was estimated by means of an inverse refraction diagram [*Hatori*, 1965 and *Iida*, 1968]. The obtained area coincided very well with the aftershock area, showing high reliability of the estimate.

On the other hand, fortunately, the survey work by the Hydrographic Office had been carried out in the adjacent sea of the epicenter just before the earthquake. Survey was repeated after the earthquake in the same area and determined the submarine crustal movement with an unprecedentedly high accuracy [*Mogi, Kawamura and Iwabuchi*, 1964]. Taking these facts into account, the Niigata tsunami is considered to be the most interesting example for our numerical experiment.

### 4a. Computing grid scheme

The wider the range in the experimental area, the more information may be obtained when the experimental values are compared with the actual ones. However, from the practical restriction of computing time and the memory capacity of a computer, the region which is treated is confined to the range from the Oga-peninsula on the north to the southwestern end of Sado Island on the south.

The adopted computing grid scheme is decided as shown in Fig. 6. The $y$-axis is taken along the general coastline in the direction N 22° E

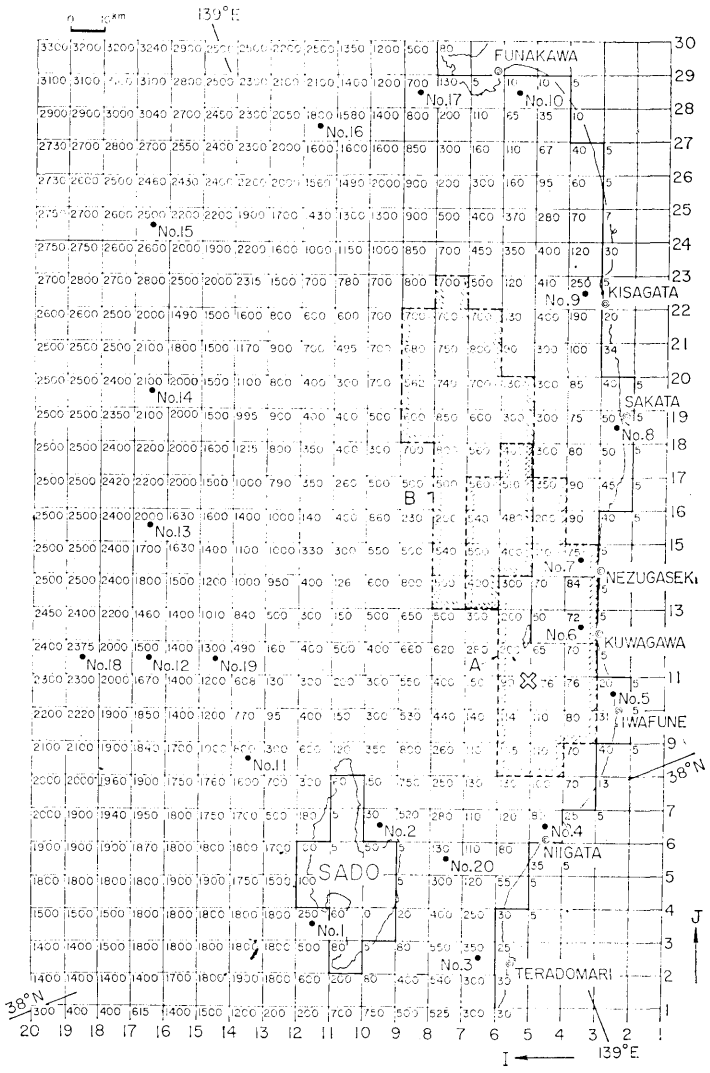


Fig. 6. Computing grid scheme for the Niigata tsunami. Numeral in each grid point shows a water depth in meters and closed circles affixed numbers are the observation points of waves. *A* shows the location and the range of the originating area of the Niigata tsunami, and *B* those when the origin is moved off the coast of Sakata. Mark ⊠ shows the earthquake epicenter.

and the $x$-axis directed seaward. The total numbers of grid points are $30\times20$ and the grid interval $\Delta s$ is 10 km. The water depth at each grid point is shown by a numeral in meters from the hydrographic chart. The grid lines drawn in bold strokes along the coast show the boundary between the land and the sea on the computation. The seaward boundary condition as mentioned in Chapter 2 is given at the

extremity of upper, lower and left sides in this grid scheme. Output of the computing results are made at points shown by numbered closed circles.

The two areas, $A$ and $B$, as shown by a broken and a chain line with hatching, are the locations of wave origins adopted in the experiment; $A$ is the actual case of the Niigata tsunami and $B$ the case removed tentatively from the location of origin. To decide the values of water elevation in the wave originating area, the computing grid is superposed over the map of submarine crustal deformation surveyed by the Hydrographic Office as shown in Fig. 7. The tsunami originating

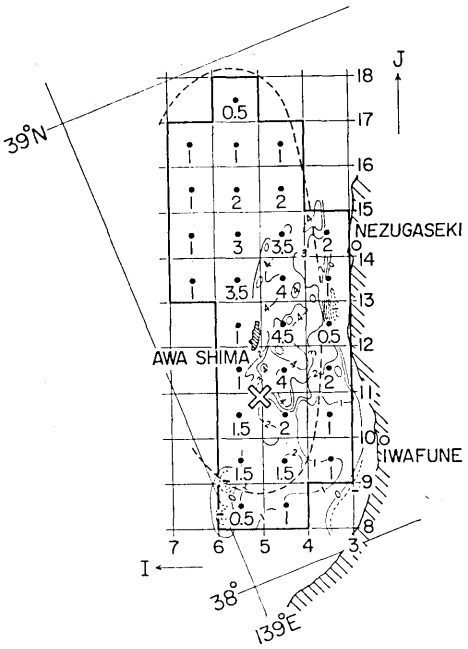


Fig. 7. Grid scheme in the tsunami originating area superposed on the map, which is shown by fine contour lines, of the submarine crustal movement surveyed by the Hydrographic office. Elliptic shape shown by a broken line is the margin of tsunami source obtained by the inverse refraction diagram (after Hatori). Grid blocks surrounded by thick solid lines are the areas of wave origin adopted in the experiment and a numeral at each block indicates the water elevation in meters given initially.

area determined by an inverse refraction diagram is an ellipse shown by a broken line. Now, as for the initial water elevations in the tsunami originating area, the approximate averaged value of submarine crustal movement in each grid block is given to its center, as shown by numerals in meters in the figure. For lack of the sounding data in the north part of the area, the values in the part are assumed to vanish gradually outward from the center. The region of subsidence in the eastern end of the deformed area is so narrow that it is neglected.

*Watanabe* [1964] proposed that the two peaks of upheaval of the sea bottom existed in the tsunami originating area. However, taking a relatively coarse spacing of grid into consideration, a model of simple mono-crest type is adopted. The water depths in most part of the

computing area are 200 m or more, therefore the waves of the period of about 7 min or more can be computed. However, as the mean depth at the nearest block to the coast becomes as shallow as 40 m in their cases, the waves whose periods are shorter than 17 min will fade away.

### 4b. Results of the numerical experiment

An experiment, where the initial water elevation was given at the location of actual wave origin of the Niigata tsunami, was carried out at first. The wave forms obtained in the various points along the coast are shown in Fig. 8. The maximum wave height appears in the neigh-

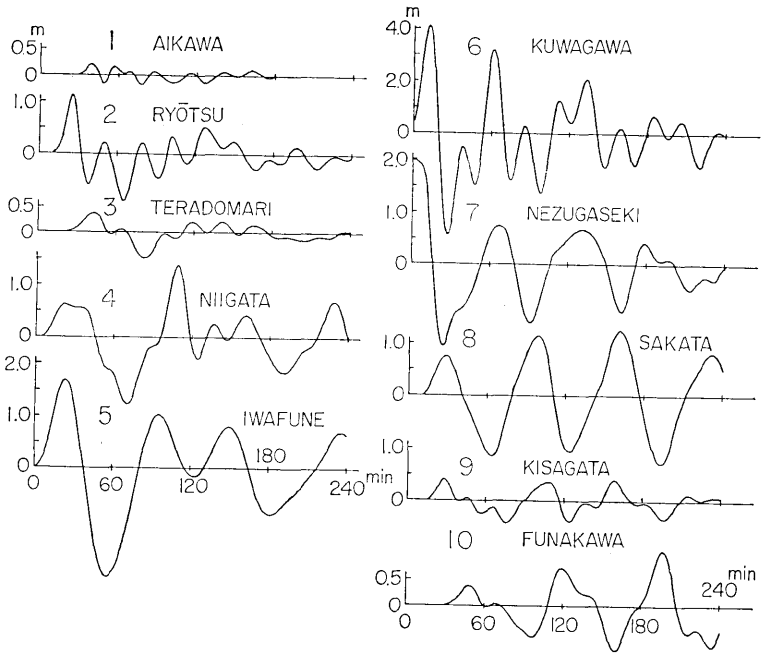


Fig. 8. Computed wave forms in various points along the coast in the case of the Niigata tsunami.

bourhood of Kuwagawa (No. 6), opposite Awa Shima, where the maximum elevation reaches as high as 4.1 m above a still water level and the short period oscillations as 20 to 28 min are dominant. In the northern and southern regions from that place, the wave amplitudes are reduced rapidly according to the distance, and the nature of the wave is considerably different from place to place. For example, the wave period at Teradomari (No. 3), the most southern place, is very short. On the other hand, at Funakawa (No. 10), the most northern place, the oscillations with long period of 60 to 80 min gradually increase their amplitudes and the third wave reaches the maximum. In the case of actual tsunami, *Nakamura and Suzuki* [1966] said that the reason for the appearance

of the maximum amplitude wave after some time had passed at Funakawa could be attributed to the development of edge waves on a shallow shelf stretch in the northern part.

It is an important matter to examine whether the wave form computed numerically coincides or not with the actual tsunami record. Unfortunately, there are few tide gage records available in the present region, due to damage caused by the earthquake. Therefore, as typical examples, only two results in Funakawa and Niigata (Matsugasaki) are shown in Fig. 9. For the grid interval is 10 km, the experimental results

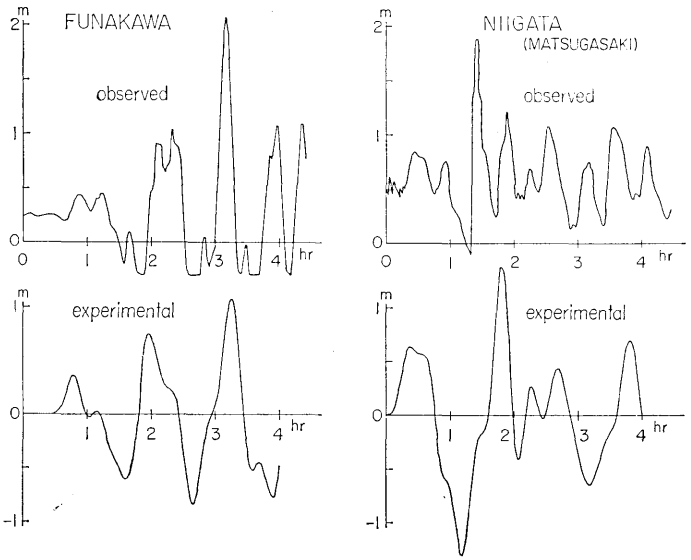


Fig. 9. Comparison between the actually observed and the experimental wave forms in the case of the Niigata tsunami.

do not indicate the values at a real coast but show the ones at rather deeper places offshore. Furthermore, since a tide gage record indicates the value in a harbor or an estuary, it may be natural that an actual observation does not completely agree with an experiment. However, looking at the figure, both results seem to coincide fairly well except for the ripple of short period. Namely, the points in which an observation coincides with an experiment are as follows; at Funakawa, the third wave is the maximum in amplitude and the periods of respective waves agree with each other, and at Niigata, the magnitude of the first falling wave is very remarkable and the second crest shows the maximum amplitude. The difference of the absolute amplitude of observed and experimental cases at Funakawa can be consistently explained. The observed amplitude should be roughly two times the experimental one,

taking into consideration the depth difference between the actual coast and the computing one as mentioned above. Similarly, at Matsugasaki, it is expected that the amplitude of observed falling wave would become small due to the effect of the shallowness of an estuary.

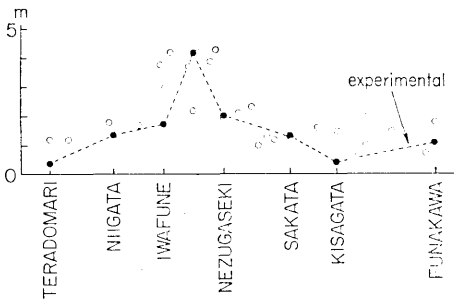


Fig. 10. Profile along the coast of the tsunami height obtained by the field investigation (open circles), and that of the maximum water elevation in the experiment (closed circles and broken line).

The distribution of the tsunami inundation heights [*Aida, et al.*, 1964] is shown by open circles in Fig. 10. The maximum heights of waves above a still water level obtained by the experiment are shown by closed circles on a broken line. The general tendency of distribution of the experimental result coincides fairly well with the one of field investigation. Taking into consideration the increase of amplitude in shallow water and the effect of run-up of waves on a sloping beach, it does not seem to be unreasonable, even if the actual observed value was two times the experimental value.

### 4c. The wave origin supposed off the coast of Sakata, (*B*)

The origins of tsunamis which occur in the Japan Sea are usually located very close to the coast, as in the case of the Niigata tsunami,

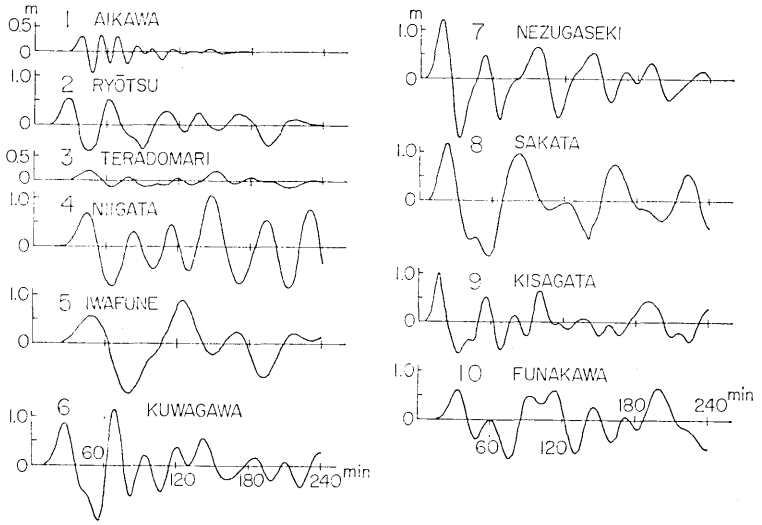


Fig. 11. Computed wave forms in various points along the coast in the case of supposed origin moved off the coast of Sakata.

so that an abnormally large amplitude appears occasionally at a localized area. If the location of the present tsunami origin were located a little seaward, the distribution of tsunami heights along the coast would have been quite different. To examine it, the tsunami origin is moved to the *B* region centered on the point about 40 km off the coast of Sakata, as shown in Fig. 6, and the same initial elevation as in the case of the Niigata tsunami is given to the center of each grid block of the originating area. The computed wave form is shown in Fig. 11.

Compared with the results in the previous section, it is seen that the wave form is changed greatly. This indicates the importance of the topographic modification of the wave form of tsunamis. The predominant period of waves in many locations has changed as is evident by comparing Fig. 11 with Fig. 8.

The distributions of the maximum height of water elevation in both cases are shown in Fig. 12, where *A* is of the Niigata tsunami shown already in Fig. 10, *B* shows the case where the origin is moved off the coast of Sakata. The distribution *B* is roughly flat from Niigata to Funakawa and the maximum height is about 1.2 m. Therefore, when such a tsunami as this case actually occurred, the maximum height would not exceed the level of 2.5 m even if the increase of amplitude near the coast was taken into consideration, in contrast to the Niigata tsunami whose maximum inundation height reached as high as 6 m.

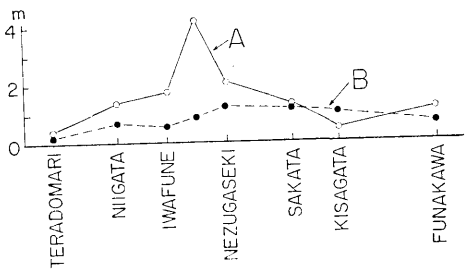


Fig. 12. Comparison for the distribution along the coast of maximum water elevation between real (*A*) and supposed (*B*) location of the tsunami origin.

### 4d. Directivity of energy radiation in a wave origin

To examine the directivity of energy radiation in the origin itself of the Niigata tsunami, a numerical experiment is carried out. The same origin as the Niigata tsunami (length; 100 km, width; 40 km) is assumed in the sea of uniform depth (500 m). The eighteen observation points are selected on a circle of a radius 90 km from the center of wave origin, and the computed wave forms in typical directions are displayed in Fig. 13. It is apparent that the amplitude and period of waves are remarkably different in each direction. Namely, the wave with small amplitude and long period is radiated in the direction of the major axis of wave origin and the one with large amplitude and short period in the minor axis.

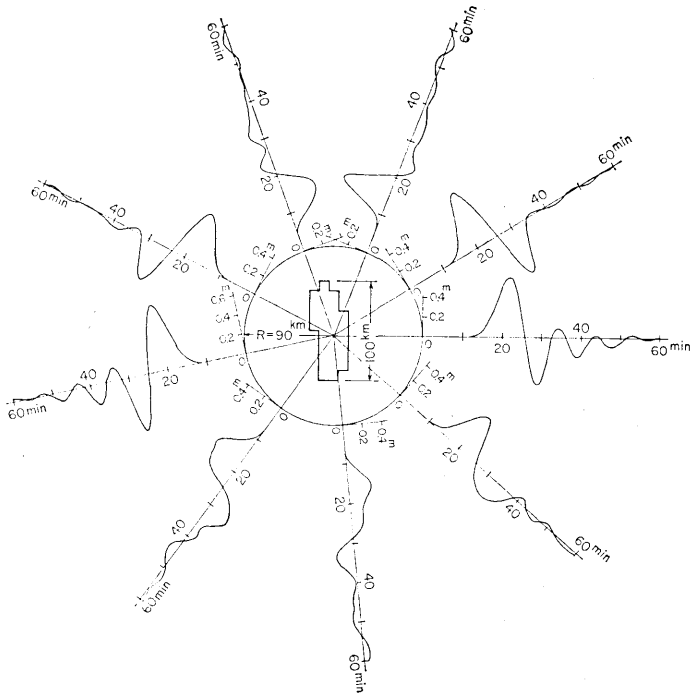


Fig. 13. Wave form radiated in every direction when it was assumed that the same origin as that of the Niigata tsunami existed on the sea at a uniform depth of 500 m.

Theoretically, the wave having a crest and a trough is to be generated. However, the waves computed in the present case are accompanied by small oscillations following a large crest and a trough. A great part of these oscillations may be caused by the process of calculation of difference equation. The energy radiation pattern, on a circle of a radius 100 km, is shown at the upper part of Fig. 14. The pattern of directivity shows such a shape as an Arabic numeral 8, in which the symmetry is a little lost since the origin is not one of complete symmetry. The ratio of radiation energy in a major direction to that in a minor one is 4.07.

The lower part of Fig. 14 shows the distribution of the amplitued of the first crest (a thick line), as well as the period of the first half wave (a broken line) at a distance of 90 km. The major axes of both patterns intersect normally with each other, showing that the longer period wave is associated with the smaller amplitude. The ratio of the major axis to the minor one in the amplitude pattern is 2.5 and that in the period pattern 1.4.

*Takahasi and Hatori* [1962] carried out an experiment for waves generated by a sudden dislocation of the bottom of elliptic shape,

in which the ratio of a long axis to a short one is equal to 3. According to their results, on a circle, a length of major axis from the center, the amplitude ratios are equal to 1.8 and 1.6, and the energy ratios 1.3 and 2.2, for 5 cm and 17.3 cm of water depths, respectively. Comparing with their results, the present tsunami origin has in itself the considerably strong directivity of energy radiation.

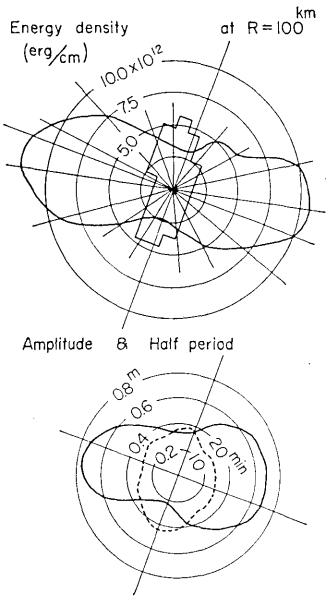


Fig. 14. Upper: Radiation pattern of energy for the Niigata tsunami source on a uniform depth sea, which is expressed by energy density in ergs per centimeter on a circle of $R=$ 100km.
Lower: Directional distribution of wave amplitudes (solid line) and half periods (broken line) in the first crest observed at observation points.

### 4e. Energy radiation pattern of the Niigata tsunami.

When a tsunami origin lies on a continental slope, the directivity of wave propagation is caused by refraction. *Miyoshi* [1968] discussed the effect of refraction when a point source of wave exists on a bottom of uniform slope, and pointed out the importance of directivity due to the shelf slope for the problem of tsunami propagation. In his case, the wave origin itself had no directivity, however, in the case of the Niigata tsunami, the wave origin had in itself remarkable directivity as mentioned in the previous section. Accordingly, the energy received at an observation point should be conspicuously different from place to place by both the effects of origin and a propagation path.

The energy radiation pattern of the Niigata tsunami is examined by calculating the wave energy at many points surrounding the wave origin. Energy is computed by taking only the first crest and the trough. Because the prolonged oscillations at coastal stations may be due to the reflection on a shelf and at shore. For simplicity, the wave energy is calculated from their maximum amplitudes and half periods by assuming sinusoidal wave form. For the observation point at the coast, the complete reflection is assumed so that 1/2 of the computed amplitude is used as the amplitude of the incident wave.

The wave energy calculated for each observation point is tabulated in Table 1, where $R$, $\varphi$ and $l$ are explained in the table. $E_n$ shown at the extreme right column is the tsunami energy passed through the portion of length $l$, and the total transmitted energy for all points

Table 1. Directional distribution of wave energy of the Niigata tsunami

| No. | $R$ (km) | $\varphi$ (°) | $l$ (km) | $E_d$ (ergs/cm) | $E_n$ (ergs) |
|---|---|---|---|---|---|
| 4 | 60 | 270 | 38 | $2.38\times10^{12}$ | $1.51\times10^{19}$ |
| 5 | 28 | 227 | 31 | 5.24 | 5.8 |
| 6 | 10 | 180 | 22 | 8.9 | 19.6 |
| 7 | 22 | 117.5 | 29 | 3.86 | 5.09 |
| 8 | 63 | 108.3 | 39 | 3.09 | 1.91 |
| 9 | 102 | 95.6 | 55 | 3.42 | 1.88 |
| 10 | 160 | 86.2 | 46 | 4.22 | 1.22 |
| 17 | 165 | 70.5 | 26 | 1.27 | 0.2 |
| 16 | 165 | 64.5 | 49 | 1.29 | 0.38 |
| 15 | 169 | 44.8 | 58 | 1.28 | 0.44 |
| 14 | 138 | 30 | 43 | 2.93 | 0.92 |
| 13 | 123 | 14 | 39 | 2.73 | 0.87 |
| 12 | 120 | 355 | 41 | 3.09 | 1.05 |
| 11 | 98 | 335 | 47 | 3.11 | 1.49 |
| 2 | 80 | 309.5 | 29 | 6.23 | 2.26 |
| 20 | 67 | 292.5 | 32 | 7.03 | 3.36 |
| | | | | | total=47.98 |

$R$: Distance from the center of tsunami origin.
$\varphi$: Direction angle measured clockwise from the line normal to the shore passing through the center of tsunami origin.
$l$: Distance from the intermediate point for a neighbouring station to the intermediate point for another station in the opposite side.
$E_d$: Energy density in ergs/cm on the circumference of the radius of 100km.
$E_n$: Energy crossing through the length "$l$".

surrounding the origin is determined to be $4.8\times10^{20}$ ergs. The energy given initially in the present model of the tsunami origin is $6.05\times10^{20}$ ergs. This value is considered to be close to the energy actually radiated by the Niigata tsunami. The energy calculated from the transmission of waves is smaller by about 20% than the initial potential energy. The discrepancy of this degree may be permissible for the following reasons; 1: the numerical experiment underestimates the true amplitude, as the short period wave is filtered out, 2: errors caused by approximating the wave form by sinusoidal one and 3: the uncertainties of the reading of the wave amplitude and of the estimation for the reflection coefficient at the coast. Now, looking through the values of $E_n$ at various points, 41% of the total energy arrives at the section of 22 km near Kuwagawa and 63.5% at the section of 82 km which include three observation poins, No. 5 to No. 7. This shows that most of the wave energy is focused toward the coast and only a little energy is radiated seaward. The

main reason may be the following, the wave origin is very close to the coast and the shape of origin is slenderly extended along the coast.

Since the observation points are not located at the same distance from the source, the energy, $E_d$, converted to that corresponding to the circle of radius 100 km, as shown by the pattern $A$ in Fig. 15. The propagation path of waves on a sloping shelf, of course, is not straight, therefore the converted values to the one at 100 km should be considered only approximate.

The strong radiation of energy toward the coast is apparent, but the seaward one is very weak. Compared with the case in a uniform depth (see Fig. 14), the decrease of radiation toward the open sea is evident. The remarkable radiation is also recognized toward Sado Island, which is considered to be the influence due to the existence of an island. A historical record said that a greater tsunami than the present one attacked Sado Island in 1833, in spite of the similar magnitude of earthquake. It might be possible that the more energy is concentrated towards Sado Island according to the location and shape of origin.

As for the case where the tsunami origin is moved off the coast of Sakata, this is similarly calculated as shown by the pattern $B$ in Fig. 15. This pattern, being in contrast to $A$, indicates that the greater part of the energy radiates seaward. It is concluded from the above

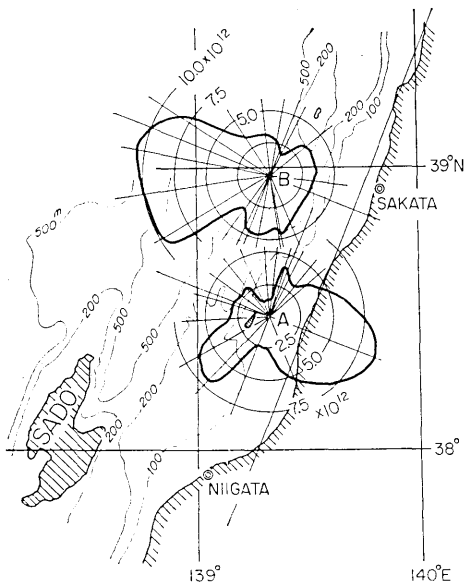


Fig. 15. Radiation pattern of energy for the Niigata tsunami ($A$), which shows a distribution of energy density converted to the propagated distance to 100km. ($B$) is the pattern for the wave origin supposed off the coast of Sakata. Unit: ergs/cm

results that the distribution of tsunami height varies drastically according to the location of wave origin.

In practice in Japan, actual tsunami energy is estimated from the wave form obtained at one or a few observation stations under the assumption of uniformity of energy radiation. *Takahasi* [1951] estimated the energy of the Sanriku tsunami of 1933 under the assumption that the energy concentrates to five of the main half waves, in the record of Ofunato. The energy estimation in the present experiment is made by summing up only two of the half waves, and still gives a reasonable result. Therefore, the waves to be adopted for the determination of tsunami energy should be confined to a first crest and a trough. Furthermore, it is strongly suggested that the consideration of an energy radiation pattern is necessary.

## 5. The Tokachi-oki tsunami of 1968

An earthquake with the magnitude 7.9 occurred on May 16, 1968. Its epicenter was located at a place 120 km southward from Erimo cape in Hokkaido. The earthquake was accompanied by a rather strong tsunami which inflicted considerable damage along the Pacific coast of the Hokkaido and Tohoku districts. It was known from the tide gage records that the tsunami began by a clear down wave in the region from the west of Erimo cape through Muroran and Hakodate to Hachinohe [*Kajiura, et al.*, 1968]. This fact suggests that a region of subsidence exists in a part of the tsunami origin. It is a very interesting problem to extract information concerning the crustal deformation from available tsunami data. An attempt in this direction is made as an example of numerical experiment.

### 5a. Grid scheme for a computation

The experimental region was confined to the range from the eastern end of Hokkaido to Oshika peninsula in Miyagi prefecture. For grid points of $30 \times 25$, the water depths are given as shown by numerals in meters in Fig. 16. As the experimental region of the present case is wider than of the previous case, the grid interval is taken to be 20 km, twice that of the Niigata tsunami. Therefore, the deterioration of the resolution is unavoidable and the discussion of short period waves are impossible.

The elliptic shape as shown by a broken line in the central part of the figure shows the tsunami origin estimated by means of an inverse refraction diagram [*Kajiura, et al.*, 1968]. In the present experiment, the region of the tsunami origin shown by the hatching line is assumed

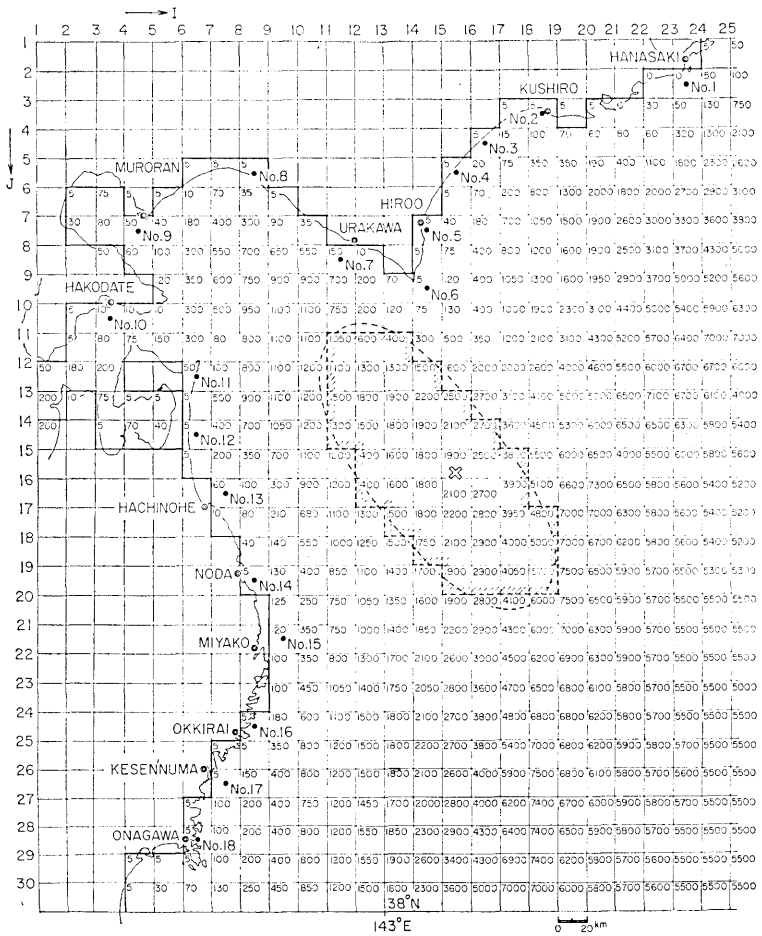


Fig. 16. Computing grid scheme for the Tokachi-oki tsunami. Numeral in each grid point shows a water depth in meters and closed circles affixed numbers are the observation points of waves. Mark ⊠ shows the earthquake epicenter. An elliptic shape shown by broken line is the tsunami originating area determined by the inverse refraction diagram. In the experiment, the area surrounded by the approximated, hatched line is adopted as the tsunami origin.

to coincide nearly with this ellipse. The information on the magnitude and the distribution of the submarine crustal deformation is not available. We can only infer the sense, up or down, of crustal deformation from the information of the initial wave of the tsunami.

Several models of tsunami origin are assumed as shown in Fig. 17. The numeral in each grid block is the water elevation in meters given initially. The common features in their models are that the area of subsidence exists at the north-west corner of the origin and the maximum elevation is 5 m. The main difference in these models is the

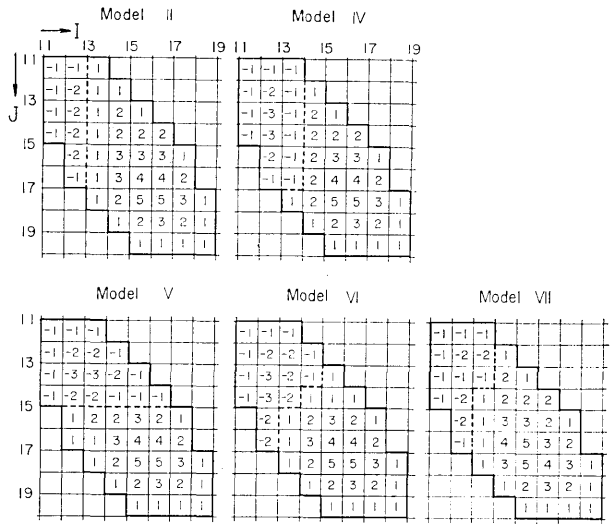


Fig. 17. Origin models adopted in the present. Numerals in grid blocks are initial water elevations in meters. Broken line shows the border line between an upheaval and a subsidence regions.

direction of border line between a subsidence and an upheaval.

The total energy assigned to the wave origin in all models is $4.06 \times 10^{21}$ ergs, which is 6.7 times that for the Niigata tsunami. From the difference of magnitude, the energy of seismic waves for the present earthquake is estimated to be 4 times the one of the Niigata earthquake. The increase of the tsunami energy relative to the seismic energy is, in this case, 1.68. This is qualitatively in agreement with *Iida's statement* [1963].

### 5b. Results of the numerical experiment

The wave forms at the observation points, as shown by numbers in Fig 16, are displayed in Fig. 18 for the case of model II. Their wave forms are slightly deformed by the filter effect due to the coarse grid mesh. The wave height and half period of the generated wave on the circumference of the wave origin are shown in Fig. 19. The wave height in the NE-SW direction is relatively large and the period is relatively long in the NNE-SSW direction in accordance with the assumed orientation of the tsunami source. The half period of wave in the direction of the major axis is about 15 min in contrast to 8 min in the direction of the minor axis. However, along the coast, the period is from 12 to 30 min as shown in Fig. 18.

In Fig. 18, the actual tide gage records with reduced scales (1/2.5 at Kushiro, Urakawa, Hachinohe and Miyako, 1/1.25 at Muroran and

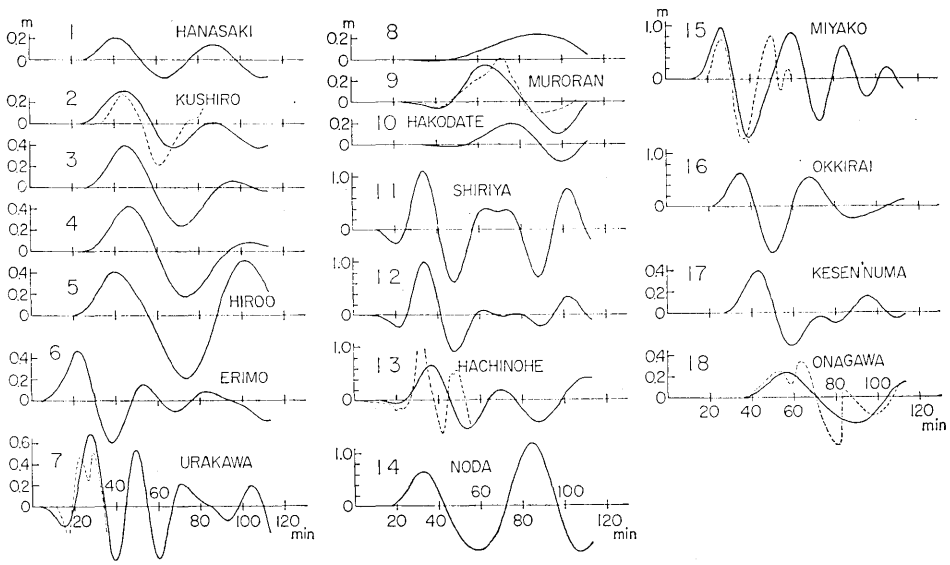


Fig. 18. Computed wave forms in various points along the coast for the case of the origin model II. Wave form shown by broken line is the tide gage record at an adjacent station, which is drawn on a scale of 1/2.5 at Kushiro, Urakawa, Hachinohe and Miyako, on a scale of 1/1.25 at Muroran and on a scale of 1/5 at Onagawa.

1/5 at Onagawa) are superposed on the experimental results by broken lines. The experimental results resemble the actual records in many cases. The tsumani record at Enoshima, located out of the bay, shows the short period as 10 min, but the experimental results show the long period of 60 min or more and agree rather well with the one at Onagawa, situated at the bay head.

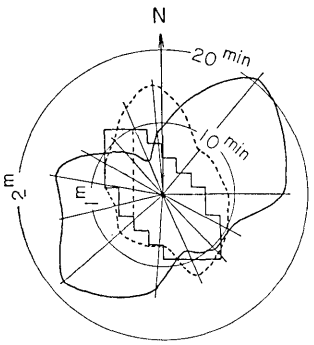


Fig. 19. Directional distribution of the amplitude (solid line) and the half period (broken line) from peak to peak of the first wave computed on the circumference close to the wave origin.

### 5c. Evaluation of proposed models

In the numerical results for five origin models shown in Fig. 17, the amplitudes of the first and second half wave, $a_1$ and $a_2$, and the ratio $a_1/a_2$ are tabulated in Table 2, together with the ones obtained from tide gage records, where the minus sign of $a_1/a_2$ corresponds to negative $a_1$. The amplitude of tide gage record is divided by 2, because the amplitude at the actual coast may be about twice the experimental results taking into account the difference in water depth. In this table, the nearest value to the actual value taken from the tide gage record

is thickly underlined and second value is finely underlined. The compatibility of the model is simply estimated by assigning 1 point to a thick underline, 0.5 points to a fine underline and the points summed up in each model as shown in the lowest line. Model II gets highest points of all $a_1/a_2$, $a_1$ and $a_2$, model VII is the next.

For the model II, IV and VII, the distribution of $a_1/a_2$, $a_1$ and $a_2$ are compared with the observed ones in Fig. 20. The waves treated at

Table 2. Comparison between the observation and the experiment with respect to the value obtained for various models.

| Station | $a_1/a_2$ | | | | | |
|---|---|---|---|---|---|---|
| | Tide Gage Record | Model | | | | |
| | | II | IV | V | VI | VII |
| Hanasaki | 1.25 | 1.23 | 1.21 | 1.34 | 1.21 | 1.25 |
| Kushiro | 0.73 | 1.39 | 1.38 | 1.67 | 1.45 | 1.42 |
| Urakawa | −0.52 | −0.267 | −0.46 | −0.50 | −0.518 | −0.348 |
| Muroran | −0.098 | −0.168 | −0.51 | −0.648 | −0.675 | −0.286 |
| Hakodate | −0.035 | −0.077 | −0.298 | −0.41 | −0.418 | −0.147 |
| Hachinohe | −0.167 | −0.086 | −0.344 | −0.411 | −0.489 | −0.114 |
| Miyako | 0.65 | 0.86 | 0.762 | 0.634 | 0.67 | 0.773 |
| Okkirai | 0.88 | 0.735 | 0.652 | 0.585 | 0.599 | 0.677 |
| Kesen'numa | 1.68 | 1.28 | 1.02 | 0.845 | 0.874 | 1.119 |
| Estimation | | 5.5 | 1 | 1.5 | 1.5 | 4 |

| Station | $a_1$ (cm) | | | | | |
|---|---|---|---|---|---|---|
| | T. G. Rec. / 2 | Model | | | | |
| | | II | IV | V | VI | VII |
| Hanasaki | 30 | 20.3 | 15.6 | 9.9 | 12.4 | 18.1 |
| Kushiro | 35 | 30.9 | 22.0 | 13.9 | 16.5 | 26.9 |
| Hiroo | 85 | 40.5 | 25.9 | −1.7 | −0.14 | 34.7 |
| Urakawa | −33 | −18.3 | −34.7 | −46.7 | −45.5 | −28.6 |
| Muroran | −2.5 | −5.74 | −14.4 | −18.7 | −19.7 | −9.3 |
| Hakodate | −1.5 | −1.52 | −5.5 | −7.5 | −8.1 | −2.8 |
| Hachinohe | −23 | −5.65 | −18.5 | −12.0 | −22.3 | −6.2 |
| Miyako | 91 | 95.3 | 72.1 | 88.7 | 74.4 | 95.8 |
| Okkirai | 78 | 64.1 | 54.5 | 58.2 | 54.9 | 64.1 |
| Kesen'numa | 47 | 39.3 | 33.5 | 34.2 | 33.1 | 39.0 |
| Estimation | | 7.5 | 1·5 | 1 | 1 | 4.5 |

(to be continued)

Table 2. (continued)

| Station | $a_2$ (cm) | | | | | |
|---|---|---|---|---|---|---|
| | T. G. Rec. / 2 | Model | | | | |
| | | II | IV | V | VI | VII |
| Hanasaki | −24 | −16.5 | −12.9 | −7.4 | −10.2 | −14.5 |
| Kushiro | −48 | −22.3 | −16.0 | −8.3 | −11.4 | −18.9 |
| Urakawa | 63 | 68.7 | 75.9 | 93.4 | 88.0 | 82.1 |
| Muroran | 26 | 34.2 | 28.3 | 28.9 | 29.0 | 32.5 |
| Hakodate | 43 | 19.7 | 18.5 | 18.3 | 19.4 | 19.1 |
| Hachinohe | 135 | 66.0 | 53.8 | 29.2 | 45.7 | 54.4 |
| Miyako | −140 | −111.0 | −94.7 | −140.0 | −111.0 | −124.0 |
| Okkirai | −90 | −87.3 | −83.6 | −99.5 | −91.9 | −94.9 |
| Kesen'numa | −28 | −30.6 | −32.5 | −40.5 | −37.9 | −34.9 |
| Estimation | | 6.5 | 2 | 1.5 | 1.5 | 2 |

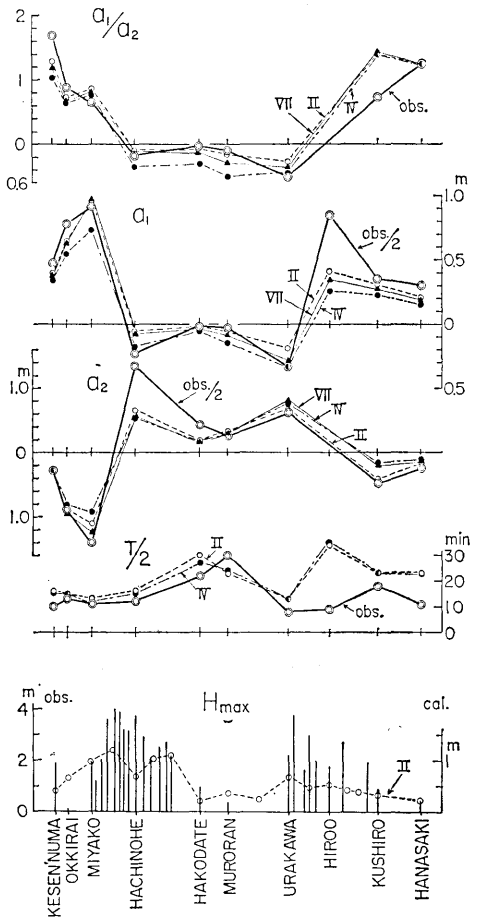


Fig. 20. Profiles of $a_1/a_2$, $a_1$, $a_2$, $T/2$ and $H_{max}$ along the coast, which are shown in contrast to the observed with the experimental values. $a_1$: the amplitude of the first half wave, $a_2$: the amplitude of the second half wave, $T/2$; the time between the peak of the first half wave and the second half wave, $H_{max}$: the maximum water elevation above still water level.

present are the leading parts of the tsunami, so that an influence due to a bay or a shelf is expected to be small. Fig. 20 verifies the considerably high compatibility of the model with reality. In the bottom of Fig. 20, the time between the first peak to the next peak, so-called a half period, $T/2$, and the maximum elevation above a still water level, $H_{max}$, are shown. The observed value of $H_{max}$, which is the inundation height above T.P. (roughly equal to M.S.L.) surveyed at the field, is amplified by the multiple reflection of bay water and by the run-up of waves at a sloping beach. Therefore it is natural that the observed value becomes a few times the calculated one. However, the general tendency of height distribution shows a rough accordance in the whole of the experimental region.

The most suitable model of tsunami origin obtained from our experiment is concluded as follows.

1. There is a region of subsidence in the northwest corner of the wave origin. Its area is $0.4\times10^4$ km$^2$ and corresponds to about 22% of the total area, $1.8\times10^4$ km$^2$.

2. The maximum upheaval is roughly about 5 m and the subsidence 2 m.

3. The border line between the subsidence and upheaval region coincides roughly with the direction N-S, on the longitude 143° E.

However, the present method can not give a unique origin model. The model should be substantiated by studies made from other view points.

It is commonly considered that the crustal movement is closely related to the earthquake mechanism. Namely, a fault line which appears on a surface of crust may coincide with one of the nodal lines of a distribution of an initial motion of earthquake. As it is said that one of the nodal lines of the Tokachi-oki earthquake is in the direction toward SSW from the epicenter, the border line between the subsidence and upheaval region in our model does not coincide with this.

*Ono, Suga and Minami* [1961] investigated the character of the initial motion observed at Sapporo in Hokkaido for earthquakes which occurred in various regions. In the region separated by the line of 143° E longitude off the south coast of Hokkaido, the initial motions of 87% of the earthquakes occurring in the eastern half were "push" in the sence, and, in the western half, those of 67% of the earthquakes were "pull". The results obtained by them may suggest that the border line of the geological structure exists along the longitudinal line of 143° E. If so, the fact that the border line between upheaval and subsidence in our model coincides with the 143° E line is very interesting.

## 6. Conclusion

The preliminary experiment on the wave propagation from a square origin in the sea of uniform water depth confirmed the possibility of obtaining reliable results as far as the long period fundamental wave was concerned.

In the numerical experiment of the Niigata tsunami, the computed wave form at the coast agreed so well with the actual tide gage record that the practical value of the present method was sufficiently proved. The directivity in radiation of the tsunami energy was discussed with respect to both that due to the wave origin itself and that which included the effect of the wave refraction on a shelf. It was clearly shown that the energy received at the coast was strikingly different, which is attributed to not only the radiation pattern of origin but also to the location and the water depth of origin on the sloping shelf. These facts seem to be important from the view point of disaster prevention and in determination of total energy of tsunami wave.

By the experiments with respect to several assumed models on the wave origin of the Tokachi-oki tsunami, the most probable model of origin was proposed. The model is as follows; the subsidence area exists in the northwest corner of the tsunami source, the border line between upheaval and subsidence corresponds to the longitudinal line of 143° E and the maximum value of upheaval is about 5 m.

To obtain higher accuracy than in the present case, more grid points will be necessary, and also the fundamental finite difference equations need to be re-examined. On the other hand, many more observations of actual wave form will be necessary to compare with the calculated results. In particular, it is desirable to obtain records in the open sea directly by tsunami recorders.

## 7. Acknowledgment

The author would like to acknowledge the useful advice and encouragement of Professor K. Kajiura, and the assistance of Mr. M. Koyama in drawing.

The numerical calculation was carried out on an IBM 360/40 at the Earthquake Prediction Observation Center, Earthquake Research Institute.

## Appendix

According to K. Kajiura, the water elevation at the center of a square origin can be obtained as follows.

A wave equation by shallow water theory is put to be

$$\nabla^2\eta-\frac{1}{c^2}\frac{\partial^2\eta}{\partial t^2}=\frac{1}{c^2}\frac{\partial w_B}{\partial t}\ ,$$

where $\eta$ is an elevation of water level, $c$ is a long wave velocity and $w_B$ is the vertical velocity of bottom deformation. If the velocity of bottom deformation is shown by

$$\begin{aligned} w_B&=H_B/\tau \qquad 0<t_0<\tau\ ,\\ &=0 \qquad\quad t_0\leq 0,\ t_0>\tau\ , \end{aligned}$$

we have the following expression by using Green's function,

$$\eta(\boldsymbol{r},\ t)=-\frac{1}{4\pi}\frac{1}{c^2}\frac{H_B}{\tau}\iint_S\{[G]_{t_0=0}-[G]_{t_0=\tau}\}ds_0\ ,$$

where Green's function $G$ is given to be

$$G(\boldsymbol{r},\ t\mid \boldsymbol{r}_0,\ t_0)=2c/\{c^2(t-t_0)^2-(\boldsymbol{r}-\boldsymbol{r}_0)^2\}^{1/2}H[c(t-t_0)-\mid \boldsymbol{r}-\boldsymbol{r}_0\mid]\ .$$

$H[\ ]$ is a step function and $\boldsymbol{r}$ a vector representing a location. The suffix "0" indicates the quantity related to a disturbed origin. An integrating area $S$ is confined to the disturbed origin. If the square origin in which a length of a side is $2a$ was assumed, the water elevation at the center ($\boldsymbol{r}=0$) is

$$\eta(0,\ t)=\frac{H_B}{\tau}[I_1-I_2]\ ,$$

where

$$I_1=t\left[1-\frac{4}{\pi}\int_0^{\varphi_d \text{ or } \varphi_{\sqrt{2}a}}\frac{1}{\cosh\varphi}\sqrt{1-\left(\frac{a}{ct}\right)^2\cosh^2\varphi}\,d\varphi H[ct-a]\right],$$

and, in $I_2$, $t$ is replaced by $(t-\tau)$. An upper limit of integral, $\varphi_d$, is determined by $d=a\cosh\varphi_d$, where $d=ct<\sqrt{2}\,a$. In the case of $ct>\sqrt{2}\,a$, $\varphi_{\sqrt{2}a}$ is employed. As for the case in which the bottom deformation occurred instantaneously, $\eta$ can be determined by taking the limit $\tau\to 0$, namely,

$$\begin{aligned}\eta(0,\ t)\simeq H_B\Bigg[1-\frac{4}{\pi}\int_0^{\varphi_d \text{ or } \varphi_{\sqrt{2}a}}\frac{1}{\cosh\varphi}-\sqrt{1-\left(\frac{a}{ct}\right)^2\cosh^2\varphi}\,d\varphi H[ct-a]\\ -\frac{4}{\pi}\left(\frac{a}{ct}\right)^2\int_0^{\varphi_d \text{ or } \varphi_{\sqrt{2}a}}\frac{\cosh\varphi}{\sqrt{1-\left(\frac{a}{ct}\right)^2\cosh^2\varphi}}d\varphi H[ct-a]\Bigg]\ .\end{aligned}$$

The right hand side of this equation can be easily integrated by a numerical method.

## References

AIDA, I., K. KAJIURA, T. HATORI, and T. MOMOI, 1964, A tsunami accompanying the Niigata Earthquake of June 16, 1964, *Bull. Earthq. Res. Inst.*, **42**, 741-780, (in Japanese).

FUKUCHI, H., and Y. ITO, 1966, On the effect of breakwaters against tsunami, *Proceedings 10th Conference on Coastal Engineering*, II, 821-839.

HATORI, T., 1965, On the tsunami which accompanied the Niigata Earthquake of June 16, 1964.—Source deformation, propagation and tsunami run-up, *Bull. Earthq. Res, Inst.*, **43**, 129-148.

IIDA, K., 1963, A relation of earthquake energy to tsunami energy and the estimation of the vertical displacement in a tsunami source, *Jour. Earth. Sci., Nagoya Univ.*, **11**, 49-67.

IIDA, K., 1968, The Niigata Tsunami of June 16, 1964, *The General Report on the Niigata Earthquake of* 1964, 97-127.

ISOZAKI, I., and S. UNOKI, 1964, The numerical computation of the tsunami in Tokyo Bay caused by the Chilean Earthquake in May, 1960, *Studies on Oceanography, Dedicated to Prof. Hidaka in Commemoration of his Sixtieth Birthday*, 389-402.

ITO, Y., K. TANIMOTO, and T. KIHARA, 1968, Digital computation on the effect of breakwaters against long-period waves (4th report), *Report of the Port and Harbour Research Institute*, **7**, No. 4, 55-83, (in Japanese).

KAJIURA, K., 1963, The leading wave of a tsunami, *Bull. Earthq. Res. Inst.*, **41**, 535-571.

KAJIURA, K., T. HATORI, I. AIDA, and M. KOYAMA, 1968, A survey of a tsunami accompanying the Tokachi-oki Earthquake of May, 1968, *Bull. Earthq. Res. Inst.*, **46**, 1369-1396, (in Japanese).

MIYOSHI, H., 1968, Re-consideration on directivity of the tsunami (I), *Zisin*, [ii], **21**, 121-138, (in Japanese).

MOGI, A., B. KAWAMURA, and Y. IWABUCHI, 1964, Submarine crustal movement due to the Niigata Earthquake in 1964, in the environs of the Awa Sima Island, Japan Sea, *Jour. Ged. Soc. Japan*, **10**, 180-186.

NAKAMURA, K., and M. SUZUKI, 1966, On the Niigata earthquake tsunami, *Research of the disaster science in the Tohoku district* (1965), 121-131, (in Japanese).

ONO, Y., M. SUGA, and K. MINAMI, 1961, Investigations on the crustal structure and seismic activity in and near Hokkaido (using the data at Sapporo D.M.O.), *Quarterly Jour. Seism.*, **26**, 39-59, (in Japanese).

REID, R., and B. BODINE, 1968, Numerical model for storm surges in Galveston Bay, *Jour. Waterways and Harbors Division, Proceedings ASCE*, **94**, 33-57.

TAKAHASI, R., 1951, An estimate of future tsunami damage along the Pacific coast of Japan, *Bull. Earthq. Res. Inst.*, **29**, 71-95.

TAKAHASI, R., and T. HATORI, 1962, A model experiment on the tsunami generation from a bottom deformation area of elliptic shape, *Bull. Earthq. Res. Inst.*, **40**, 873-883, (in Japanese).

UENO, T., 1965, Numerical computations for the Chilean Earthquake Tsunami, *Oceanographical Magazine*, **17**, 87-94.

WATANABE, H., 1964, Generation mechanism of tsunamis caused by Niigata Earthquake, *Bull, Coastal Oceanography*, **3**, No. 2, 31-37, (in Japanese).

## 29. 津波伝播の数値実験—1964年新潟津波および1968年十勝沖津波

地震研究所　相田　勇

日本近海の津波波源から海岸までの津波伝播の問題は，種々興味あるところであるが，今まで実験的に取扱つた例はなかつた．ここでは，数値実験の方法でこの問題を取扱つた．

方法は，基礎微分方程式を差分方程式に変換し，計算格子上の各点の水位分布，流量分布を交互に計算する通常の方法である．

予備実験として，正方形波源が，一定水深の海にある場合について行ない，格子間隔の疎い場合，細かい場合の比較を行なつた．

続いて新潟津波について，水路部で測られた波源附近の海底の変動が瞬間的に起つたものとして，日本海岸の各地に到達する津波を求めた．検潮記録との比較で，実験波形はかなりよく一致し，また全体の波高分布も実測とよく一致する．波源自身のエネルギー放射の指向性についても調べたが，波源は8字形の指向性を持つている．実際には陸側にのみ強い指向性を示し，沖には非常に弱くなる．これは陸棚傾斜によるものと解される．

十勝沖津波について数個の波源モデルが仮定され，それぞれについて実験が行なわれた．各地の検潮記録と比較した結果，最も適当と思われるモデルが求められた．それによると，波源域の北西隅に沈降地域があつて，沈降と上昇地域の境界は，ほぼ143° Eの線の上にある，隆起量の最大は約5 m位である，などが推定される．